Research Article

Roland Tolulope Loto* and Asamaige Ogaga

Inhibition effect of the synergistic properties of 4-methyl-norvalin and 2-methoxy-4-formylphenol on the electrochemical deterioration of P4 low carbon mold steel

https://doi.org/10.1515/eng-2020-0002
Received Jun 08, 2019; accepted Nov 03, 2019

Abstract: Study of the synergistic inhibition properties of the combined admixture of 4-methyl-norvalin and 2-methoxy-4-formylphenol (non-toxic organic compounds) on the corrosion of P4 low carbon mold steel in 1.5 M H_2SO_4 and HCl solution was performed with weight loss measurement, potentiodynamic polarization and optical microscopy analysis. Results obtained showed the inhibition efficiency of the admixed compound performed above the value for effective corrosion inhibition at very low concentrations in H_2SO_4 solution. However, from mid concentration to the highest concentration studied, the inhibition efficiency of the compound was above 85% from electrochemical tests. In HCl solution the inhibition efficiency of the compound was well above 80% and 90% for weight loss and polarization tests at all concentration studied. Anodic corrosion inhibition mechanism was determined for the compound in H_2SO_4 according to Freundlich and Frumkin adsorption isotherms due to weak Van der Waals attraction between the inhibitor molecules and the steel's surface. The mechanism of corrosion inhibition in HCl was calculated to be cathodic type according to Langmuir isotherm model. Morphological images of inhibited and non-inhibited steel surfaces significantly contrast each other though the extent of deterioration was much severe for the steel from H_2SO_4 solution.

Keywords: corrosion; pitting; steel; inhibition; acid

1 Introduction

Corrosion, the chemical or electrochemical deterioration of engineering materials due to reaction with their environments has been a recurring problem for decades. The problem is responsible for the huge financial cost required for repair, replacement and maintenance of industrial parts, components, structures, equipment's etc. that are prone to deterioration [1, 2]. Corrosion of metallic alloys is of importance due to their extensive industrial applications especially in environments where aqueous corrosion reactions are present. Carbon steel combines excellent mechanical properties with good formability, availability and low cost as a result it is the most widely used steel. However, it has very weak resistance to corrosion, thus the need for cost effective replacement with steels of higher corrosion resistance in addition to effective corrosion control method. P4 low carbon mold steel, a tool grade steel with extensive application in plastics processing industry has improved thermal conductivity, high levels of toughness and hardness, machinability and good corrosion resistance [3]. At temperature beyond 165°C hydrogen chloride gas permeates from PVC, combining with atmospheric moisture and resulting in HCl acid. This and other highly corrosive media can corrode the steel [4]. However, the presence of Cr and Mo at 5% and 0.4% composition within this steel offers improved corrosion resistance compared to the traditional carbon steels [5–7]. The limited presence of chromium causes the formation of passive protective film against the attack of corrosive anions while Mo offers improved resistance to localized corrosion especially pitting [8–12]. In addition to this, use of chemical compounds known as corrosion inhibition can complement the protective ability of the alloying elements on the low carbon mold steel. Corrosion inhibitors tend to counteract the electrochemical action of corrosive species in aqueous environments. Depending on the category of the inhibitor they act by film formation, selective precipitation and/ or alteration of the

***Corresponding Author: Roland Tolulope Loto:** Department of Mechanical Engineering, Covenant University, Ota, Ogun State, Nigeria; Email: tolu.loto@gmail.com
Asamaige Ogaga: Department of Mechanical Engineering, Covenant University, Ota, Ogun State, Nigeria

Table 1: Composition (wt. %) of PLCS

Element Symbol	Cu	Si	Cr	Mn	P	S	C	Mo	Fe
% Composition (LCMS)	0.25	0.25	5	0.4	0.03	0.03	0.12	0.4	92

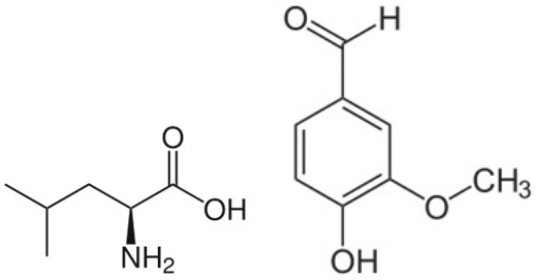

(a) (b)

Figure 1: Molecular structure of (a) 4-methyl-norvalin and (b) 2-methoxy-4-formylphenol

corrosive environment [13]. Research on green corrosion inhibitors shows it acts through film formation on carbon steels with good inhibition protection [14–17]. In contribution to research on corrosion prevention through appropriate material selection and chemical control, this research aims to study the synergistic combination effect of 4-methyl-norvalin and 2-methoxy-4-formylphenol organic derivatives on the corrosion of P4 low carbon mold steel in dilute H_2SO_4 and HCl solution.

2 Experimental method

P4 low carbon mold steel (PLCS) sourced from the open market gave nominal (wt.%) composition shown in Table 1, after analysis at the Materials Characterization Laboratory, Department of Mechanical Engineering, Covenant University, Ota, Ogun State, Nigeria. The low carbon mold steel is of cylindrical configuration (diameter, 1.6 cm). The steel was machined, sectioned to average thickness of 0.6 cm, and grinded with silicon carbide papers (80, 320, 600, 800 and 1000 grits) before washing with distilled water and acetone. 4-methyl-norvalin purchased from Sigma Aldrich, USA is a white powdery substance with molecular formula of $C_6H_{13}NO_2$ and molar mass of 131.17 g/mol. Its molecular structure is shown in Figure 1(a). 2-methoxy-4-formylphenol is a phenolic aldehyde organic powdery compound with the molecular formula of $C_8H_8O_3$ and molar mass of 152.15g/mol. Its molecular structure is shown in Figure 1(b). Their combined admixture (MTH) in ratio 1:1 was prepared into 0.5g, 1g, 1.5g, 2g, 2.5g and 3g which were each added to 200 ml of 1.5 M H_2SO_4 and HCl solution to give volumetric concentrations (%) of 0%, 0.25%, 0.5%, 0.75%, 1.0%, 1.25% and 1.5% MTH. Potentiodynamic polarization analysis was performed at 30°C with a three-electrode system within glass cell containing 200 mL of the electrolyte solution at specific MTH concentrations. The electrodes which consist of resin embedded PLCS electrodes with exposed surface area of 1.13 cm^3 were connected to Digi-Ivy 2311 potentiostat. Polarization plots obtained at scan rate of 0.0015 V/s between potentials of –2 V and +1 V. Weight loss measurement of PLCS specimens was performed in 200 mL of the acid solution for 240 h at 24 h interval. Graphs of corrosion rate and inhibition efficiency versus exposure time were plotted from the data obtained during the exposure hours. Optical images of corroded and inhibited PLCS morphology were analysed after weight loss with Omax trinocular metallurgical microscope to produced photomicrographs with magnification of ×40.

3 Results and discussion

3.1 Weight-loss analysis

Inhibition study of specific concentrations of MTH inhibiting compound on PLCS corrosion in 1.5M H_2SO_4 and HCl solution was performed for 240 h. Data for weight-loss (ω_L), corrosion rate (C_R), and MTH inhibition efficiency (ξ_F) after at 240 h of exposure are shown in Table 2. Figures 2(a) and 2(b) show the plots of PLCS corrosion rate and MTH inhibition efficiency versus exposure time in H_2SO_4 and HCl solution. The corrosion rate of PLCS at 0% MTH in H_2SO_4 solution [Figure 2(a)] was significantly higher than the values obtained for PLCS at specific MTH/H_2SO_4 solutions due to the electrochemical action of SO_4^{2-} species within the electrolyte. The corrosion rate value at 24 h (10.96 mm/y) increased significantly to 22.98 mm/y at 120 h, after which it remained generally stable till 168 h before declining to 18.70 mm/y at 240 h. The presence of MTH compound at lower volumetric concentrations (0.25% - 0.75% MTH) significantly reduced the corrosion rate values of PLCS in comparison to values obtained at 0% MTH. However, the corrosion rates of PLCS

Table 2: Experimental data from weight loss measurement at 240 h for PLCS corrosion in 1.5 M H_2SO_4 and HCl (0% - 1.5% MTH)

H_2SO_4				
Samples	**MTH Vol. Concentration (%)**	**Weight Loss (g)**	**Corrosion Rate (mm/y)**	**Inhibition Efficiency (%)**
A	0	3.033	18.70	0
B	0.25	2.443	15.07	19.44
C	0.5	1.939	11.96	36.07
D	0.75	1.729	10.66	42.99
E	1.0	0.160	0.99	94.73
F	1.25	0.159	0.98	94.77
G	1.5	0.133	0.82	95.61
HCl				
Samples	**MTH Vol. Concentration (%)**	**Weight Loss (g)**	**Corrosion Rate (mm/y)**	**Inhibition Efficiency (%)**
A	0	1.280	7.89	0
B	0.25	0.046	0.28	96.41
C	0.5	0.037	0.23	97.14
D	0.75	0.057	0.35	95.53
E	1.0	0.079	0.48	93.86
F	1.25	0.020	0.12	98.44
G	1.5	0.041	0.26	96.77

at these concentrations continued to increase significantly from onset to values between 15.07 and 10.66 mm/y at 240 h. These values show MTH compound between 0.25% and 0.75% MTH has no inhibiting action on the corrosion of PLCS other than to interfere with the corrosion reaction mechanisms. Further increase in MTH volumetric content to values between 1% and 1.5% drastically decreased the corrosion rate of PLCS to values between 2.95 mm/y and 2.47 mm/y at 24 h, and 0.99 mm/y and 0.82 mm/y at 240 h. This observation is due to the presence of sufficient molecules of MTH to counteract the electrochemical action of SO_4^{2-}anions on PLCS surface. The observation also shows MTH inhibiting action in H_2SO_4 is concentration dependent. Figure 3(a) shows the inhibiting action of MTH in H_2SO_4 at 1% to 1.5% MTH concentration is generally stable after 72 h of exposure till 240 h. The MTH compound performed more effectively in HCl solution with inhibition efficiency above 90% at all concentrations studied [Figure 3(b)] throughout the exposure hours. The inhibiting action of MTH also proves to be more stable in HCl than in H_2SO_4 throughout the exposure hours. It is also observed that the performance of MTH compound is independent of concentration. PLCS at 0% MTH/HCl [Figure 2(b)] deteriorated rapidly with the corrosion rate reaching 1.280 mm/y at 240 h. Though this value is quite lower than the value obtained in H_2SO_4, it nevertheless signifies active surface deterioration of the steel.

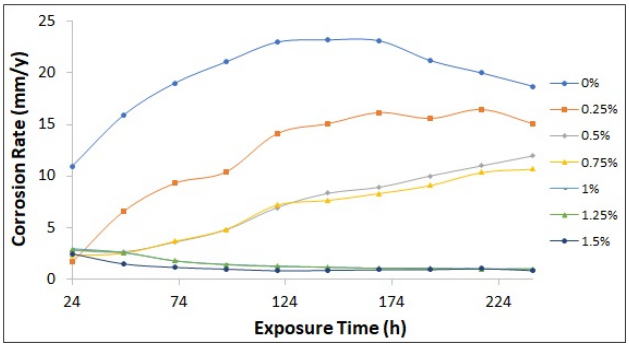

(a)

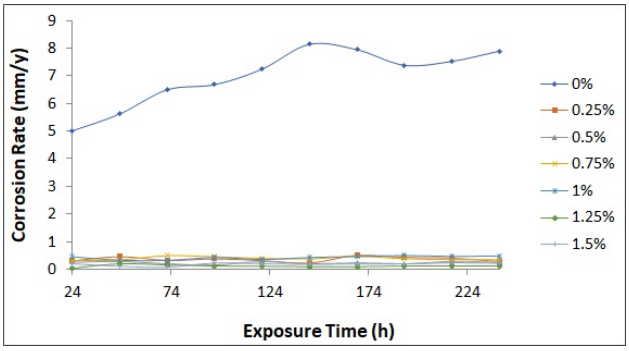

(b)

Figure 2: Plots of PLCS corrosion rate versus exposure time at 0% - 1.5% MTH inhibiting compound (a) in 1.5M H_2SO_4 and (b) in 1.5M HCl

Table 3: Calculated results of potentiodynamic polarization plots for PLCS in 1.5M H_2SO_4 and HCl solution at 0% - 1.5% MTH concentration

H_2SO_4									
Sample	**MTH Vol. Conc. (%)**	**PLCS C_R (mm/y)**	**MTH ξ_F (%)**	**C_I (A)**	**C_J (A/cm^2)**	**C_P ($V_{Ag/AgCl}$)**	**R_p (Ω)**	**B_c (V/dec)**	**B_a (V/dec)**
A	0	9.48	0	1.80E−03	8.93E−04	−0.287	21.51	−10.450	0.572
B	0.25	6.80	28.32	1.29E−03	6.40E−04	−0.243	33.18	−9.474	9.962
C	0.5	5.23	44.85	9.90E−04	4.93E−04	−0.199	54.10	−9.089	13.670
D	0.75	4.58	51.71	8.67E−04	4.31E−04	−0.221	63.80	−9.949	41.560
E	1	1.05	88.92	1.99E−04	9.90E−05	−0.201	172.60	−8.198	15.580
F	1.25	0.73	92.33	1.38E−04	6.85E−05	−0.236	145.30	−9.428	14.180
G	1.5	0.68	92.87	1.28E−04	6.37E−05	−0.239	200.70	−9.191	40.250
HCl									
Sample	**MTH Vol. Conc. (%)**	**PLCS C_R (mm/y)**	**MTH ξ_F (%)**	**C_I (A)**	**C_J (A/cm^2)**	**C_P ($V_{Ag/AgCl}$)**	**R_p (Ω)**	**B_c (V/dec)**	**B_a (V/dec)**
A	0	3.24	0	6.13E−04	3.05E−04	−0.458	62.15	−8.001	0.320
B	0.25	0.50	84.54	2.57E−04	1.28E−04	−0.462	300.10	−7.993	2.740
C	0.5	0.49	84.79	2.53E−04	1.26E−04	−0.488	292.90	−10.280	2.233
D	0.75	0.39	88.06	1.98E−04	9.86E−05	−0.567	279.60	−8.196	3.476
E	1	0.53	83.76	2.70E−04	1.34E−04	−0.512	308.30	−11.190	3.516
F	1.25	0.48	85.23	2.45E−04	1.22E−04	−0.564	291.01	−10.520	4.450
G	1.5	0.41	87.31	2.11E−04	1.05E−04	−0.610	283.60	−8.862	4.200

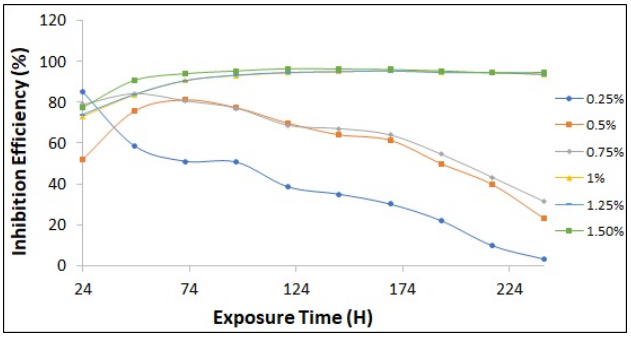

(a)

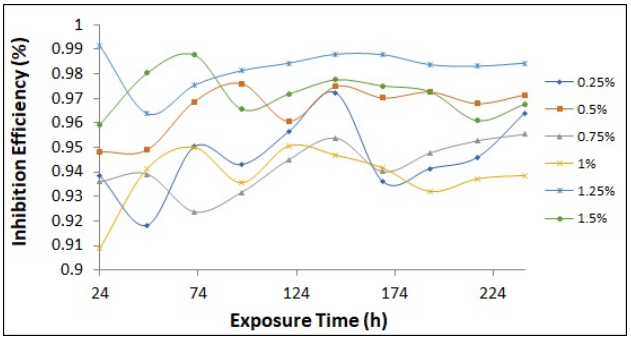

(b)

Figure 3: Plots of PLCS inhibition efficiency versus exposure time at 0% - 1.5% MTH inhibiting compound (a) in 1.5M H_2SO_4 and (b) in 1.5M HCl

3.2 Potentiodynamic polarization studies

Corrosion polarization studies performed on PLCS in 1.5M H_2SO_4 and HCl solution at 0%, 0.25%, 0.5%, 0.75%, 1%, 1.25% and 1.5% MTH inhibiting compound resulted in the potentiodynamic polarization plots shown in Figure 4 and 5. Table 3 shows the polarization data. In H_2SO_4 solution, addition of MTH at 0.25% concentration shifts the corrosion potential of PLCS in the anodic direction from $-0.287V_{Ag/AgCl}$ (0% MTH) to $-0.243V_{Ag/AgCl}$. This phenomenon is due to partial surface coverage of PLCS by MTH inhibitor molecules which counteracts the electrochemical action of SO_4^{2-} anionic species. The change in corrosion potential corresponds to change in corrosion rate from 9.48 mm/y (0% MTH) to 6.80 mm/y (0.25% MTH) resulting in very low inhibition efficiency of 28.32%. Further increase in MTH concentration caused alternating shifts in corrosion potential within anodic inhibition processes. Increased in inhibition efficiency also occurred, attaining an optimal value of 92.87 at 1.5% MTH concentration. The visible decrease in corrosion rate values corresponds to decrease in corrosion current and increase in polarization resistance with increase in inhibitor concentration. Observation of the Tafel slopes shows variation in MTH concentration has not significant influence on the cathodic reaction process compared to the anodic counterpart. This supports the discussion of anodic inhibition from observation of changes in corrosion potential values.

The polarization plot in Figure 4 shows similar cathodic polarization behavior confirming that the mecha-

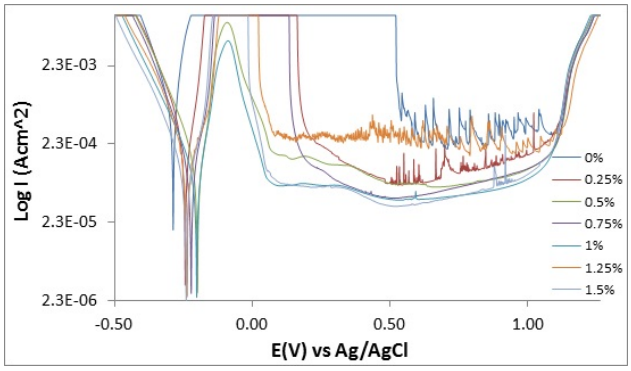

Figure 4: Polarization plots for PLCS at 0% - 1.5% MTH/1.5 M H_2SO_4 solutions

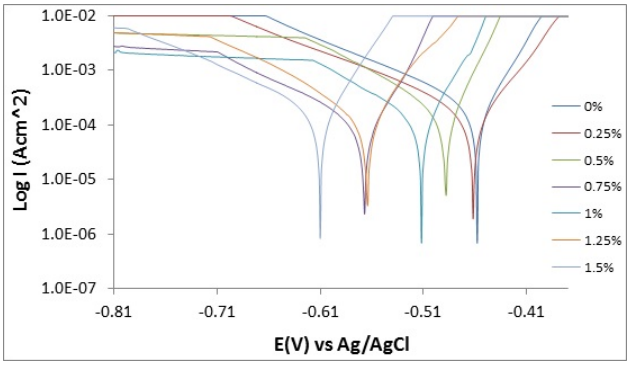

Figure 5: Polarization plots for PLCS at 0% - 1.5% MTH/1.5 M HCl solutions

nisms of hydrogen evolution and oxygen reduction reaction are not affected. Similar anodic polarization behavior before passivation processes also occurred. The passivation plot of PLCS at 0% MTH passivated briefly from 0.49V to 1.11V, producing a short passivation range before failure. This phenomenon is associated with pitting corrosion behavior due to the formation of microscopic pits at sites where the passive films breaks. The passive film on the plot shows acute instability from the visible current transients. The passivation region of the polarization plots of PLCS from 0.25% MTH to 1.5% MTH increased significantly compared to the plot for PLCS at 0.25% MTH due to formation of protective film by MTH molecules on PLCS surface. This hindered the formation of corrosion pits. The increase in passivation region signifies higher corrosion resistance of PLCS in the presence of MTH concentrations. The visible current transients on the passivation plot of PLCS at 0% MTH synonymous with unstable passivation decreased significantly at 0.25% MTH, beyond which it completely disappeared due to stability of the passive film.

The corrosion polarization behavior of PLCS in HCl/MTH solution [Figure 5] contrasts its behavior in H_2SO_4 acid media. Cathodic shift in corrosion potential was observed with increase in MTH concentration, compared to the anodic shift in H_2SO_4. The shift is associated with selective precipitation of MTH molecules on PLCS surface whereby the cathodic reaction mechanism of the corrosion process is inhibited. Changes in cathodic Tafel slope values confirm this proposition. While the corrosion rate of PLCS in HCl is relatively smaller than the value obtained in H_2SO_4 at 0% MTH, it significantly differs from the values obtained at specific concentrations of MTH. The largest difference in corrosion potential of PLCS (in both acids) from 0% MTH shows MTH ia an anodic type inhibitor in H_2SO_4 and cathodic type in HCl [18].

3.3 Adsorption isotherm and corrosion thermodynamics

The nature of intermolecular reaction among protonated MTH molecules in interaction with PLCS surface can be further understood through mathematical models known as adsorption isotherms. Adsorption isotherms are graphical plots between the amounts of MTH molecules adsorbed on the surface of PLCS at constant temperature. The plots explain the sorption type or adhesion of MTH molecules to PLCS surface with respect to corrosion inhibition. In H_2SO_4 solution the intermolecular reaction and adsorption of protonated MTH obeyed the Freundlich isotherm according to equation 1 and 2 with correlation coefficient of 0.8680, and the Frumkin isotherms with correlation coefficients of 0.8530 according to equation 3. Figure 6(a) and 6(b) show the Freundlich and Frumkin isotherm plots.

$$\theta = KC^n \tag{1}$$

$$\log \theta = \mathrm{n} \log C + \log K_{ads} \tag{2}$$

n is a constant with respect to the characteristics of adsorbed MTH molecule, K_{ads} is the adsorption-desorption equilibrium constant representing the intermolecular strength of the adsorbed layer. Freundlich isotherm describes the relationship between adsorbed molecules, their interaction (repulsion or attraction) and influence on the adsorption mechanism [19, 20].

$$\log \left[C_{MTH} \times \left(\frac{\theta}{1-\theta} \right) \right] = 2.303 \ \log K_{ads} + 2\alpha\theta \tag{3}$$

Frumkin isotherm assumes total coverage of PLCS surface at high MTH concentrations for non-homogeneous materials and the effect of lateral interaction is significant. This involves considering the functional sites on the adsorbent surface.

Table 4: Data for Gibbs free energy (ΔG^{o}_{ads}), surface coverage (θ) and equilibrium constant of adsorption (K_{ads}) for MTH adsorption on PLCS in H_2SO_4 and HCl solution

H_2SO_4				
Specimen	**MTH Conc. (M)**	**Surface Coverage (θ)**	**Equilibrium Constant of adsorption (K_{ads})**	**Gibbs Free Energy, ΔG (Kjmol^{-1})**
A	0	0	0	0
B	8.82E−03	0.194	0.239	−6.41
C	1.76E−02	0.361	0.431	−7.87
D	2.65E−02	0.430	0.504	−8.26
E	3.53E−02	0.947	1.097	−10.18
F	4.41E−02	0.948	1.087	−10.16
G	5.29E−02	0.956	1.088	−10.16
HCl				
Specimen	**MTH Conc. (M)**	**Surface Coverage (θ)**	**Equilibrium Constant of adsorption (K_{ads})**	**Gibbs Free Energy, ΔG (Kjmol^{-1})**
A	0	0	0	0
B	8.82E−03	0.964	3040.01	−29.83
C	1.76E−02	0.971	1924.94	−28.69
D	2.65E−02	0.955	807.52	−26.54
E	3.53E−02	0.939	433.03	−25.00
F	4.41E−02	0.984	1427.87	−27.95
G	5.29E−02	0.968	565.06	−25.66

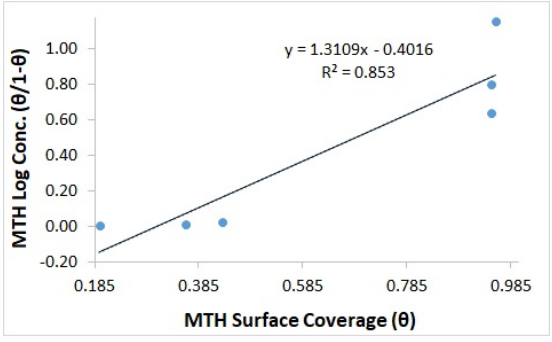

(a)

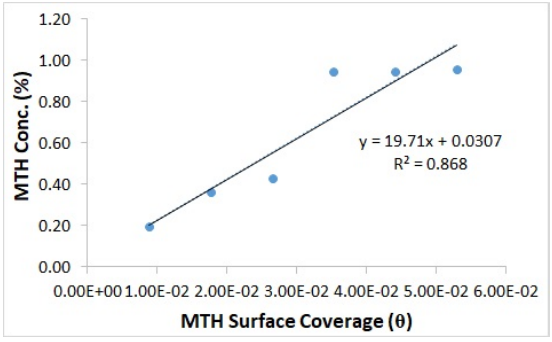

(b)

Figure 6: (a) Freundlich isotherm plot, and (b) Frumkin isotherm plot

In HCl, MTH obeyed the Langmuir isotherm with correlation coefficient of 0.9977 according to equation 4. Figure 7 shows the Langmuir isotherm plots.

$$\theta = \left[\frac{K_{ads}C_{MTH}}{1 + K_{ads}C_{MTH}}\right] \tag{4}$$

The Langmuir isotherm assumes the intermolecular reaction on the metal surface is constant, the value Gibbs free energy is independent of the degree of molecular coverage and there is no lateral interaction effect resulting from the molecular reaction of adsorbates on the value of Gibbs free energy [21].

The physiochemical nature and adsorption strength of MTH intermolecular reaction on PLCS surface was determined from thermodynamic calculations. Data on Gibbs free energy, ΔG^{o}_{ads} evaluated from equation 5 is shown in Table 4 [22].

$$\Delta G_{ads} = -2.303RT\log[55.5K_{ads}] \tag{5}$$

where 55.5 is the molar concentration of water in the solution, R is the universal gas constant, T is the absolute temperature and K_{ads} is the equilibrium constant of adsorption. K_{ads} for MTH adsorption on PLCS in H_2SO_4 solution was determined from the Freundlich isotherm due to its higher correlation coefficient value while K_{ads} for MTH adsorption on PLCS in HCl solution was determined

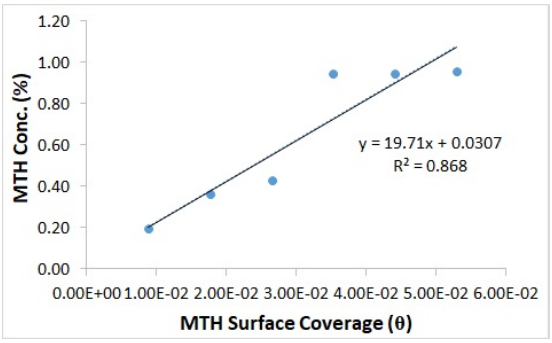

Figure 7: Langmuir isotherm plot

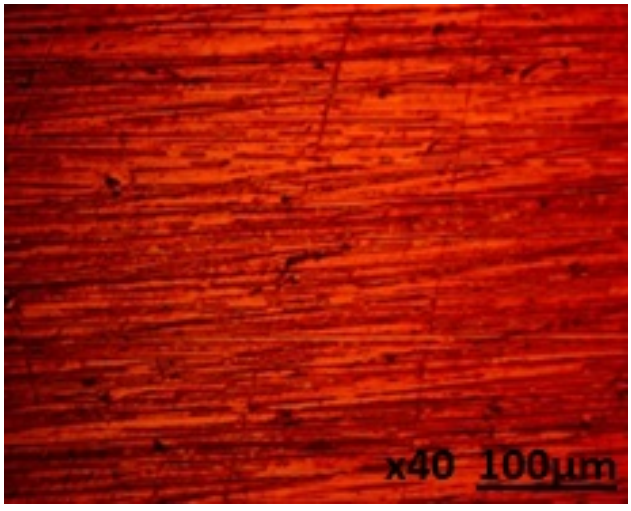

Figure 8: Morphology of PLCS before corrosion test

from the Langmuir isotherm. The negative values of ΔG^o_{ads} show the spontaneity and stability of the adsorption mechanism. In H_2SO_4 solution the ΔG^o_{ads} values obtained depicts physisorption adsorption mechanism. ΔG^o_{ads} values obtained for MTH inhibition in HCl solution shows physiochemical adsorption mechanism whereby molecular attraction and corrosion inhibition is through weak Van der Waals forces, and mild electrostatic attraction and covalent bonding.

3.4 Optical microscopy studies

Microscopic observations of PLCS (mag. ×40) before corrosion and after corrosion at 0% and 1.5% MTH in both acids are shown from Figure 8 to Figure 10(b). The morphological deterioration of PLCS at 0% MTH in H_2SO_4 and HCl solution where quite extensive due to the debilitating action of SO_4^{2-} and Cl^- anions [Figure 9(a) and 9(b)]. However, extent of deterioration in Figure 9(a) is much more than Figure 9(b) which confirms the corrosion rate results from potentiodynamic polarization test. While the deterioration in Figure 9(a) appears to be general surface deterioration in addition to the presence of numerous micro pits, the deterioration in Figure 9(b) shows the presence of fewer but more defined micro pits due to the electrochemical action of chlorides whose corrosive actions tends to be localized on PLCS surface. At 1.5% MTH the deteriorating effect of the anionic species on PLCS subsided due to the inhibiting action of protonated MTH molecules as shown in Figure 10(a) and Figure 10(b). The visible micro pits prevalent in Figure 9(a) substantially reduced in Figure 10(a) in addition to a less deteriorated morphology, while the micro pits shown in Figure 9(b) where generally absent in Figure 10(b). The few corrosion pits in Figure 10(b) appears

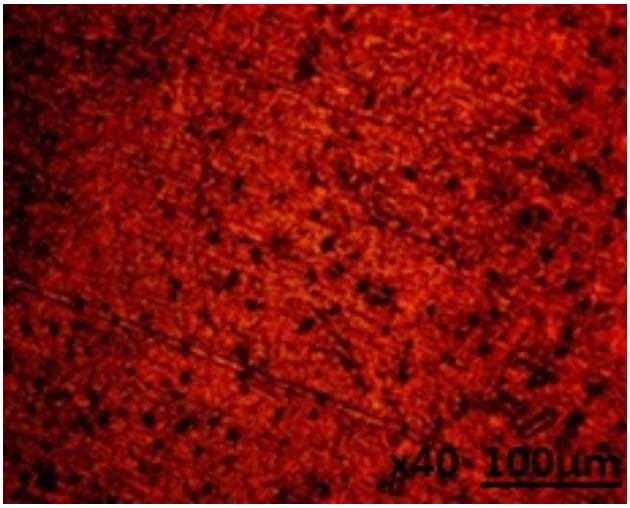

(a)

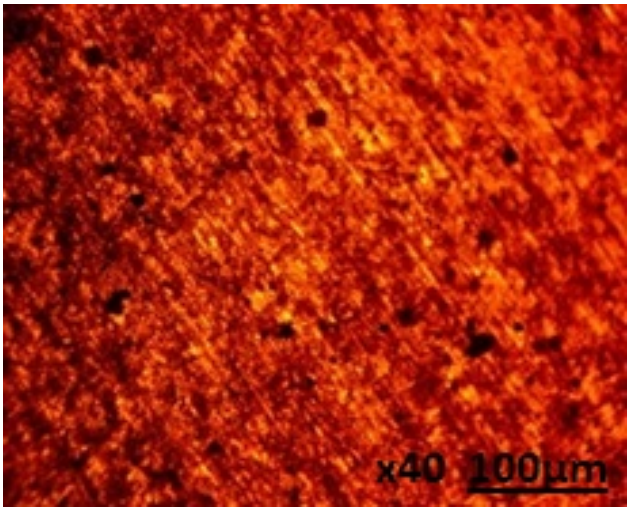

(b)

Figure 9: Morphology of PLCS after corrosion at 0% MTH (a) 1.5 M H_2SO_4 and (b) 1.5 M HCl

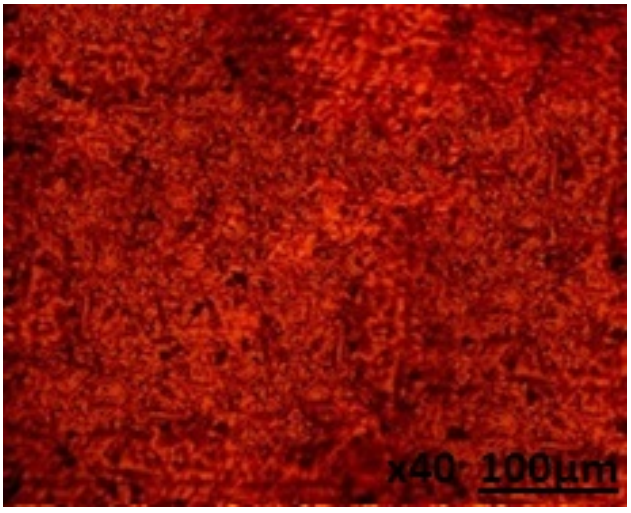

(a)

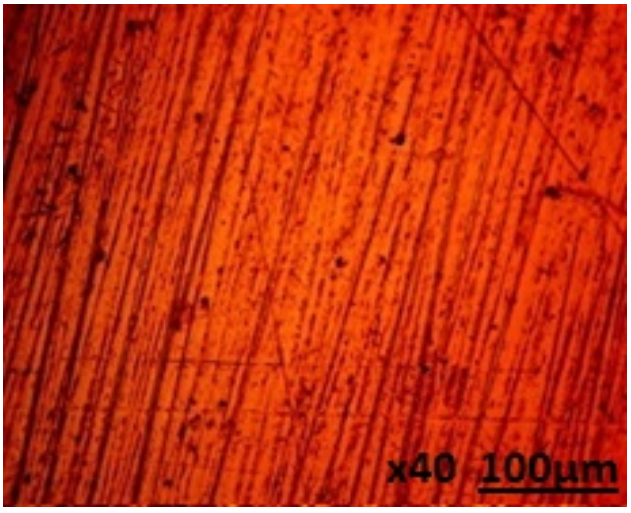

(b)

Figure 10: Morphology of PLCS after corrosion at 1.5% MTH (a) 1.5 M H_2SO_4 and (b) 1.5 M HCl

shallow due to the inhibition action of MTH which arrested the formation of corrosion pits in Figure 9(b).

4 Conclusion

The combined admixture of 4-methyl-norvalin and 2-methoxy-4-formylphenol effectively inhibited the corrosion of P4 low carbon mold steel in H_2SO_4 and HCl solution. Observation of the inhibition efficiency values with respect to exposure time shows the inhibition performance of the organic compound was concentration and time dependent in H_2SO_4 while in HCl its performance is independent of these parameters. Calculated results from statistical derivations of the adsorption isotherms shows the adsorption of the inhibitor molecules on the adsorbent steel surface were exceptionally weak indicating surface coverage through film formation is the inhibition mode in H_2SO_4 while in HCl statistical derivation shows physiochemical interaction in addition to weak chemical bonding occurred between the inhibitor molecules and the ionized steel surface.

Acknowledgement: The author acknowledges Covenant University Ota, Ogun State, Nigeria for the sponsorship and provision of research facilities for this project.

References

[1] Akinyemi OO, Nwaokocha CN, Adesanya AO. Evaluation of corrosion cost of crude oil processing industry. J Eng Sci Technol. 2012;7(4):517-528.
[2] Loto RT. Study of the corrosion S32101 duplex and 410 martensitic stainless steel for application on oil refinery distillation systems. J Mater Res Techn. 2017;6(3):203-212.
[3] P4 Tool Steel (UNS T51604) - Low-Carbon Mold Steel. [2018-06-02]. www.azom.com/article.aspx?ArticleID=6236.
[4] Sammt K, Sammer J, Geckle J, Liebfahrt W. Development trends of corrosion resistant plastic mould steels. 6th International Tooling Conference. Karlstad; 2012:339-348.
[5] Osarolube E, Owate IO, Oforka NC. Corrosion behavior of mild and high carbon steels in various acidic media. Sci Res Essays. 2008;3(6):224-228.
[6] Möller H, Boshoff ET, Froneman H. The corrosion behaviour of a low carbon steel in natural and synthetic seawaters. J South Afr Inst. Min Metall. 2006;106:585-592.
[7] Song Y, Jiang G, Chen Y, Zhao P, Tian Y. Effects of chloride ions on corrosion of ductile iron and carbon steel in soil environments. Sci Rep. 2017;7:6865. doi.org/10.1038/s41598-017-07245-1.
[8] Fahim A, Dean AE, Thomas MDA, Moffatt EG. Corrosion resistance of chromium steel and stainless steel reinforcement in concrete. Mats & Corr. 2018;1-17. doi.org/10.1002/maco.201709942.
[9] Olsson COA, Landolt D. Passive films on stainless steels—chemistry, structure and growth Electrochim Acta. 2003;48(9):1093-1104.
[10] Shih CC, Shih CM, Su YY, Su LHJ, Chang MS, Lin SJ. Effect of surface oxide properties on corrosion resistance of 316L stainless steel for biomedical applications. Corros Sci. 2004; 46(2):427-441.
[11] Hazza MI, El-Dahshan ME. The effect of molybdenum on the corrosion behaviour of some steel alloys. Desalination. 1999;95(2):199-209.
[12] Mesquita TJ, Chauveau E, Mantel M, Kinsman N, Nogueira RP. Influence of Mo alloying on pitting corrosion of stainless steels used as concrete reinforcement. Rem: Rev Esc Minas. 2013;66(2). doi.org/10.1590/S0370-44672013000200006
[13] Dariva CG, Galio AF. Corrosion Inhibitors – Principles, Mechanisms and Applications, Developments in Corrosion Protection. IntechOpen. 2014;365-379. doi.org/10.5772/57255.

[14] Jafari H, Akbarzade K, Danaee I. Corrosion inhibition of carbon steel immersed in a 1 M HCl solution using benzothiazole derivatives. Arabian J Chem. 2014. doi.org/10.1016/j.arabjc.2014.11.018.
[15] Loto CA, Loto RT. Effect of dextrin and thiourea additives on the zinc electroplated mild steel in acid chloride solution. Int J Elect Sci. 2013;8(12):12434-12450.
[16] Loto CA, Loto RT, Popoola API. Electrode potential monitoring of effects of plants extracts addition on the electrochemical corrosion behaviour of mild steel reinforcement in concrete, Int J Elect Sci. 2011;6(8):3452-3465.
[17] Loto RT. Surface coverage and corrosion inhibition effect of rosmarinus officinalis and zinc oxide on the electrochemical performance of low carbon steel in dilute acid solutions. Results Phys. 2018;8:172-179.
[18] Loto RT, Loto CA. Effect of p-phenylediamine on the corrosion of austenitic stainless steel type 304 in hydrochloric acid. Int J Elect Sci. 2012;7(10):9423-9440.
[19] Arivoli S., Kalpana K., Sudha R., Rajachandrasekar T.E., Comparative study on the adsorption kinetics and thermodynamics of metal ions onto acid activated low cost carbon, Electron. J. Chem., 2007, 4(4), 238-254.
[20] Ashish K, Quraishi MA. Investigation of the effect of disulfiram on corrosion of mild steel in hydrochloric acid solution. Corros Sci. 2011;53(4):1288-1297.
[21] Guidelli R. Adsorption of molecules at metal electrodes. Kowski JL, Ross PN (eds.), NewYork: VCH Publishers lnc.;1992:1.
[22] Aharoni C, Ungarish M. Kinetics of activated chemisorption. Part 2. Theoretical models. J Chem Soc Faraday Trans. 1977;73:456-464.